Earthquakes and Structures, *Vol. 16, No. 2 (2019) 129-139*
DOI: https://doi.org/10.12989/eas.2019.16.2.129

A method for analyzing the buckling strength of truss structures

Yi Pan[1], Renqi Gu[1], Ming Zhang[*1], Gerry Parke[2] and Alireza Behnejad[2]

[1]*School of Civil Engineering, Southwest Jiaotong University, Chengdu 610031, China*
[2]*Department of Civil and Environmental Engineering, University of Surrey, Guildford GU2 7XH, UK*

(Received December 12, 2018, Revised January 17, 2019, Accepted January 23, 2019)

Abstract. This paper develops a new method for estimating the elastic-plastic buckling strength of the truss structures under the static and seismic loads. Firstly, a new method for estimating the buckling strength of the truss structures was derived based on the buckling strength of the representative member considering the parameters, such as the structure configurations, boundary conditions, etc. Secondly, the new method was verified through the buckling strength estimation and the finite element method (FEM) analysis of the single member models, portal frame models and simple truss models. Finally, the method was applied to evaluate the buckling strength of a simple truss structure under seismic load, and the failure loads between the proposed method and the FEM were analyzed reasonably. The results show that the new method is feasible and reliable for structure engineers to estimate the buckling strengths of the truss structures under the static loads and seismic loads.

Keywords: buckling strength; representative member; truss structures; static load; seismic load

1. Introduction

Stability problems are extremely significant of spatial truss structure and have been extensively studied in many papers. Rozvany (1996) investigated the relations between global buckling and local buckling by analyzing the system stability constraints of the structure. Tada and Suito (1998) analyzed the dynamic post-buckling behavior of a plane parallel chord truss structures and a double-layer space truss structure based on the assumption that the mass distributes in the member. BEN-TAL *et al*. (2000) introduced a linear buckling model of the stability problems for truss based on the strain energy of the structure. Dou *et al*. (2013) studied the elastic out-of-plane buckling load of circular steel tubular truss arches by using the static equilibrium approach. Halpern and Adriaenssens (2015) investigated the nonlinear elastic in-plane buckling behavior of shallow truss arches by calculating the equivalent moment of inertia and equivalent area of truss cross sections. Madah and Amir (2017) studied the local buckling and the global buckling of trusses with geometrical imperfection based on co-rotational beam formulation using the gradient-based method of moving asymptotes. Wattanamankong *et al*. (2017) studied the behavior of lateral buckling of truss structures and evaluated the lateral buckling coefficient by using buckling of a bar with intermediate compressive forces. Tugilimana *et al*. (2018) analyzed the global stability of a truss topology structure by calculating the total potential energy using Green Lagrange strain tensor. The above studies analyzed the stability of the truss structure by calculating the stability parameters of the structure.

The practices indicated that it is difficult to analyze the stability of the truss structure by calculating the stability parameters with the increasing of members. Thus, some researchers analyzed the stability of the truss structure based on the FEM. Bi (2016) analyzed the linear buckling, geometric nonlinear stability and nonlinear stability of large-span steel tubular truss based on the FEM. Konkong *et al*. (2017) investigated the lateral buckling of a cold-formed steel truss structure by the experimental test and FEM analysis. Sui *et al*. (2018) analyzed the elastic global buckling and elastic critical local buckling of the double-shell octagonal lattice truss composite structures by using the FEM. Unfortunately, most of them only analyzed the linear stability or the elastic stability of the structure by using the FEM, and they seldom consider the elastic-plastic buckling load of the truss structure.

Meanwhile, some researchers studied the buckling behavior of the truss under the earthquake. Ramesh and Krishnamoorthy (2005) performed the inelastic post-buckling analysis of truss structures by the Dynamic Relaxation method. Thai and Kim (2011) carried out the nonlinear inelastic time-history analysis of truss structures under earthquake with considering the buckling and inelastic post buckling. Dai *et al*. (2013) researched the local buckling and global buckling of two gymnasiums of steel space structures by investigating the damage of 2013 M7.0 Lushan earthquake in China. However, most of researchers considered the linear buckling strength or inelastic post-buckling of the truss structure under earthquake, and they seldom took into account the elastic-plastic buckling strength of the truss structure under earthquake.

Accordingly, the present study aims to propose a buckling strength, the elastic-plastic buckling strength in another word, analysis method of the truss structure. In particular, the present works focuses on (i) demonstrating the proposed buckling strength analysis by analyzing the

∗Corresponding author, Ph.D.
E-mail: zhangming@home.swjtu.edu.cn

http://www.techno-press.com/journals/eas&subpage=7 ISSN: 2092-7614 (Print), 2092-7622 (Online)

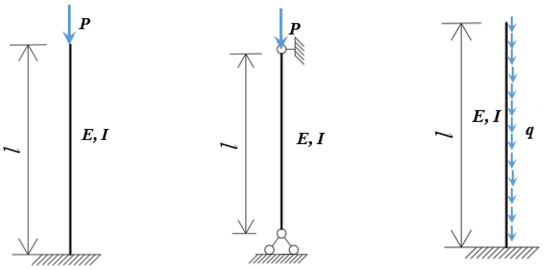

(a) Member under concentrated load with rigid connection

(b) Member under concentrated load with pin connection

(c) Member under gravity with rigid connection

Fig. 1 Member, with different connections, under different load

buckling strength of the single member models, the portal frame models and the simple truss models; (ii) ensuring that the proposed formulations consider the effect of the plastic; (iii) applying the proposed buckling strength analysis method to analyze the buckling strength of a simple truss under earthquake. Therefore, the paper is organized as follows: Section 1 introduces studies about buckling analysis, and a method of buckling strength analysis is proposed in Section 2. Several examples of the buckling strengths analysis are given in Section 3 to verify the method. Buckling strength analysis of simple truss under earthquake are given in Section 4. Conclusions and future research directions are given in Section 5.

2. A method of buckling strength analysis

The buckling strength of structures is affected by many factors and is difficult to be calculated. Thus, factors relating to buckling strength are introduced firstly. Then the relationship between the representative member and the truss structure is discussed. Finally, the buckling strength of structures is analyzed which is based on the linear elastic analysis of the structures, the linear buckling analysis of the representative member and the elastic buckling analysis of the representative member.

2.1 Factors relating to buckling strength

Taking the theory of Euler's member buckling for example to explain the factors related to the buckling strength, the buckling strength N_{Euler} of member under concentrated load, as shown in Fig. 1(a) and Fig. 1(b), could be calculated based on Eq. (1) and the buckling strength $(ql)_{\mathrm{cr}}$ of member under gravity, as shown in Fig. 1(c), could be calculated based on Eq. (2).

$$N_{\mathrm{Euler}} = \frac{\pi^2 EI}{(\mu l)^2} \tag{1}$$

$$(ql)_{\mathrm{cr}} = \frac{\pi^2 EI}{(\mu l)^2} \tag{2}$$

where E is Young's modulus of the member, I is the weakest second moment of inertia of the member's cross-section, l is the length of the member and μ is a parameter corresponding to the boundary of the member and the form of load.

The parameter I and l are related to the configuration of the structure. Once the configuration of the structure is defined, the parameter I could be calculated in terms of the section of the member and the parameter l could be calculated in terms of the coordinates of the member's nodes. The values μ of the members under concentrated load with the rigid connection and pin connection are 2 and 1, respectively. And the value μ of the member under gravity with the rigid connection is 1.12.

Consequently, the buckling strength is related to the boundary of the structure by comparing the buckling strength of the member under concentrated load with the rigid connection and pin connection. In addition, the buckling strength is related to the form of the load by comparing the buckling strength of the member under concentrated load and gravity. In summary, the parameters, the configuration, the boundary conditions of structure and the form of load, have important influence on the buckling strength.

2.2 The relationship between the representative member and the truss structure

The representative member (Kato 2014), introduced in Section 2.3, is defined by considering the structure configuration, boundary conditions, load distribution, connections between members and nodes and geometric imperfections as well as material and geometric nonlinearity. Therefore, the representative member is the key member in a structure, and whose failure may lead to local buckling, progressive collapse, and even a whole structure collapse. Moreover, the buckling strength of the representative member can be regarded as the key reference value to analyze the buckling strength of the truss structure.

2.3 Linear elastic analysis

The fundamental information on stress, strain and displacement of the structure could be obtained by linear elastic analysis (Long *et al*. 2001, Zhang *et al*. 2019). And an equation for linear elastic analysis is obtained as follows

$$[K_{\mathrm{E}}]\{D\} = \lambda\{P\} \tag{3}$$

where $[K_{\mathrm{E}}]$ is the material and geometrical linear stiffness matrix of the structure, $\{D\}$ is the displacement vector, λ is a factor of loading increment and $\{P\}$ is the load vector considering the load distribution of the design load and the pertinent load combinations. And the displacement vector $\{D\}$ increases linearly with the increase of λ in linear elastic analysis. When the value λ equals to 1, the fundamental responses of the structure on nodal displacement $\{D_{0i}\}$, nodal bending moments $\{M_{0i}\}$ and axial force N_{0i} of the ith element are calculated under design load. Here, it should be noted that the characteristic magnitude of the load $\{P\}$ is difficult to describe, as that the load may vary on the structure with a specified distribution. For convenience, the maximum vertical load P_0 at node or the maximum vertical load intensity q_0 per unit area is defined as the representative load to represent the characteristic magnitude of the load $\{P\}$.

Importantly, a member whose absolute value of normal stress, as given by Eq. (4), is the largest among all members in a structure under compression is defined as the representative member of the structure (Kato 2014).

$$|N_{0i}/A_i| \tag{4}$$

where N_{0i} and A_i respectively denote the axial force of the i th member under the design load and the cross-sectional area of the ith member.

Under the design load, the axial force of the representative member is defined as N_0, and the load applied on it is expressed as P_{0R}. Moreover, the representative member is considered to yield faster than any other members under the compression when the value of λ is increased from 0 to a special amount.

2.4 Linear buckling analysis of the representative member

An equation based on the matrix displacement method for linear stability analysis is shown as follows (Long *et al.* 2001)

$$([K_{\mathrm{E}}] - \lambda[K_{\mathrm{s}}])\{D\} = \{0\} \tag{5}$$

where $[K_{\mathrm{s}}]$ is the geometric stiffness matrix expressing the effect of initial stresses exerted under the design load, and λ is a factor of loading increment and should be satisfied in the eigenvalue problem of Eq. (5). A set of $\{\lambda\}$ could be obtained by solving the eigenvalue problem of Eq. (5). The lowest positive eigenvalue is defined as the first buckling load factor and it is expressed as $\lambda_{\mathrm{cr}}^{\mathrm{lin}}$.

Consequently, the linear buckling strength of the representative member $P_{\mathrm{0R\_cr}}^{\mathrm{lin}}$ could be calculated in terms of Eq. (6). And the linear axial buckling force of the representative member $N_{\mathrm{0cr}}^{\mathrm{lin}}$ is defined by using the first buckling load factor $\lambda_{\mathrm{cr}}^{\mathrm{lin}}$ and the axial force N_0 which is the axial force of the representative member under the design load, as shown in Eq. (7). Similarly, the linear buckling load of the structure could be calculated by Eq. (8). It means that the structure is linear buckling when the value of the representative load P_0 or q_0 reaches $\lambda_{\mathrm{cr}}^{\mathrm{lin}} P_0$ or $\lambda_{\mathrm{cr}}^{\mathrm{lin}} q_0$.

$$P_{\mathrm{0R\_cr}}^{\mathrm{lin}} = \lambda_{\mathrm{cr}}^{\mathrm{lin}} P_{\mathrm{0R}} \tag{6}$$

$$N_{\mathrm{0cr}}^{\mathrm{lin}} = \lambda_{\mathrm{cr}}^{\mathrm{lin}} N_0 \tag{7}$$

$$P_{\mathrm{0cr}}^{\mathrm{lin}} = \lambda_{\mathrm{cr}}^{\mathrm{lin}} P_0 ; \;\; q_{\mathrm{0cr}}^{\mathrm{lin}} = \lambda_{\mathrm{cr}}^{\mathrm{lin}} q_0 \tag{8}$$

2.5 Elastic buckling analysis of the representative member

Based on the geometrical nonlinear of the structure and material linear analysis, elastic buckling load of the representative member, $P_{\mathrm{0R\_cr}}^{\mathrm{el}}$, could be estimated (Kato 2014). The elastic buckling load $P_{\mathrm{0cr}}^{\mathrm{el}}$ is generally less than the corresponding load obtained by linear buckling analysis, as the effect of geometric imperfection and semi-rigidity at connection shall be considered in the elastic buckling analysis and both of them will reduce the elastic buckling load.

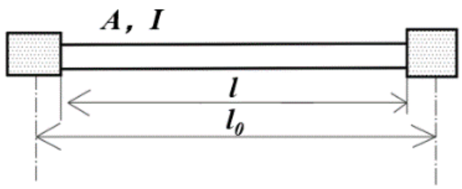

(a) Rigid connection

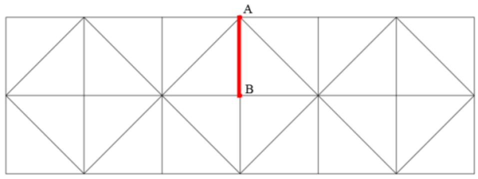

(b) Connection in structure

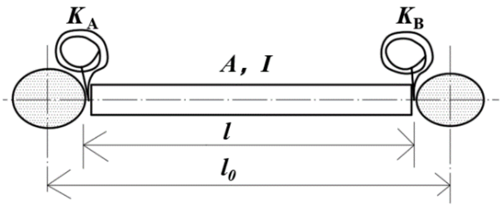

(c) Semi-rigid connection

Fig. 2 Connection of the representative member

However, not only the imperfection magnitude but also the corresponding distribution over the structure is difficult to ascertain, and the ratio of buckling load reduction as the exact quantity is difficult to compute. Here, the maximum imperfection of the structures w_0 is regarded as 1/1000 for the long span of the structures according to the steel fabrication in AIJ (Architectural Institute of Japan, JASS6 1996). And one node of the representative member is assumed to be given an imperfect of w_0 and almost no imperfection is assumed at other nodes.

The connection of the representative member is often assumed to be the rigid connection in the structure, no rotation and displacement in the connection as shown in Fig. 2(a), and it is convenient to analyze the elastic buckling load of the representative member. However, the connection of the representative member in red and which is bolded, in Fig. 2(b) is regarded as semi-rigidity in the structure since the deformation of the member which is connected with the representative member will lead to the nodal rotation or displacement that will result in the reduction of the buckling load of the representative member. The connection of the representative member in Fig. 2(b) could be simplified as a semi-rigidity connection whose stiffness is between that of pin connection and rigidity connection, as shown in Fig. 2(c), according to the theory of structural mechanics. The K_{A} and K_{B} are the bending stiffness at the connection node A and node B.

Taking into account the geometric imperfections and semi-rigidity at connections, the elastic buckling load of the representative member $P^{\mathrm{el}}_{\mathrm{0R\_cr}}$, utilizing the linear buckling load of the representative member $P^{\mathrm{lin}}_{\mathrm{0R\_cr}}$, could be evaluated as the following equation.

$$P^{\mathrm{el}}_{\mathrm{0R\_cr}} = \alpha \cdot P^{\mathrm{lin}}_{\mathrm{0R\_cr}} \tag{9}$$

$$\alpha = \alpha_0 \cdot \beta \tag{10}$$

where α_0 and β respectively denote the reduction ratio of the elastic buckling load due to the geometric imperfection and semi-rigid connection.

Based on the values θ of the semi-rigidity as shown in Fig. 2(c), the α_0 and β could be defined as follows.

$$\alpha_0 = \frac{P^{\mathrm{el}}_{\mathrm{0R\_cr(imp)}}(\theta = 0)}{P^{\mathrm{lin}}_{\mathrm{0R\_cr}}(\theta = 0)} \tag{11}$$

$$\beta = \frac{P^{\mathrm{el}}_{\mathrm{0R\_cr}}(\theta = 1)}{P^{\mathrm{el}}_{\mathrm{0R\_cr}}(\theta = 0)} \tag{12}$$

where $\theta = 0$ denotes that the connection is completely rigid as shown in Fig. 2(a), $\theta = 1$ denotes that the connection is semi-rigidity as shown in Fig. 2(c) and the connection could rotate under the bending moment, $P^{\mathrm{el}}_{\mathrm{0R\_cr(imp)}}(\theta = 0)$ means the elastic buckling load of the representative member considering the geometric imperfection and completely rigid connection, while $P^{\mathrm{lin}}_{\mathrm{0R\_cr}}(\theta = 0)$ means the linear buckling load of the representative member considering the rigid connection without the imperfection. The $P^{\mathrm{el}}_{\mathrm{0R\_cr}}(\theta = 1)$ means the elastic buckling load of the representative member only considering the semi-rigid connection, while $P^{\mathrm{el}}_{\mathrm{0R\_cr}}(\theta = 0)$ means the elastic buckling load of the representative member only considering the completely rigid connection.

Consequently, the elastic buckling load of the representative member $P^{\mathrm{el}}_{\mathrm{R\_0cr}}$ is expressed in terms of α or $\lambda^{\mathrm{el}}_{\mathrm{0cr}}$ in Eq. (13). Similarly, the elastic buckling load of the truss structure $P^{\mathrm{el}}_{\mathrm{0cr}}$ is expressed in terms of α or $\lambda^{\mathrm{el}}_{\mathrm{0cr}}$ in Eq. (14).

$$P^{\mathrm{el}}_{\mathrm{0R\_cr}} = \alpha \cdot P^{\mathrm{lin}}_{\mathrm{0R\_cr}} = \lambda^{\mathrm{el}}_{\mathrm{0cr}} \cdot P_{\mathrm{0R}} \tag{13}$$

$$P^{\mathrm{el}}_{\mathrm{0cr}} = \alpha \cdot P^{\mathrm{lin}}_{\mathrm{0cr}} = \lambda^{\mathrm{el}}_{\mathrm{0cr}} \cdot P_0 \tag{14}$$

$$\lambda^{\mathrm{el}}_{\mathrm{0cr}} = \alpha_0 \cdot \beta \cdot \lambda^{\mathrm{lin}}_{\mathrm{cr}} \tag{15}$$

where $P^{\mathrm{el}}_{\mathrm{0cr}}$ and $\lambda^{\mathrm{el}}_{\mathrm{0cr}}$ mean the elastic buckling load and elastic buckling loading factor considering the geometric imperfection and semi-rigid connection, respectively. The structure will happen to elastic buckling when the representative load P_0 or q_0 reaches $\lambda^{\mathrm{el}}_{\mathrm{cr}} P_0$ or $\lambda^{\mathrm{el}}_{\mathrm{cr}} q_0$.

2.6 Evaluation of buckling strength of the structures based on the representative member

The buckling strength of the structures is calculated based on the generalized slenderness ratios and the axial strength of the representative member.

2.6.1 Generalized slenderness ratio of the representative member

When the α and $P^{\mathrm{el}}_{\mathrm{0R\_cr}}$ have been calculated, the elastic buckling axial force of the representative member, $N^{\mathrm{el}}_{\mathrm{0cr}}$, could be approximately evaluated by Eq. (16) considering the geometric imperfection and semi-rigid connection.

$$N^{\mathrm{el}}_{\mathrm{0cr}} = \alpha \cdot N^{\mathrm{lin}}_{\mathrm{0cr}} = \alpha \cdot \lambda^{\mathrm{lin}}_{\mathrm{cr}} \cdot N_0 \tag{16}$$

Referring to the definition of the slenderness ratio of an ordinary column in a high-rise building (Kato 2014), the generalized slenderness ratio Λ_0 of the representative member could be given as follows.

$$\Lambda_0 = \sqrt{\frac{N_{\mathrm{y}}}{\alpha \cdot N^{\mathrm{lin}}_{\mathrm{0cr}}}} \tag{17}$$

$$N_{\mathrm{y}} = A_0 \cdot \sigma_{\mathrm{y}} \tag{18}$$

where N_{y} means the yield force of the representative member under an axial load; A_0 means the cross section area of the representative member; σ_{y} means the yield strength of the representative member. To avoid joint failure, the strength and rigidity of the connection are assumed to be large enough compared with the representative member.

2.6.2 Axial strength of the representative member

In most case, the region subjected to buckling is almost the same as that subjected to yielding (Kato 2014). Therefore, a member in a truss under compression is assumed to buckle and yield at the same location. And the axial strength N_{cr} of the representative member can be approximately evaluated if the analysis of N_{cr} is based on an appropriate column strength curve (Kato 2014). According to the Dunkerley's formulation for column strength curve (Eq. (19)) (Architectural Institute of Japan 2010, Ogawa *et al.* 2008), the axial strength of the representative member could be calculated by Eq. (20) in terms of the generalized slenderness ratio Λ_0.

$${\Lambda_0}^2 \cdot \left(\frac{k_{\mathrm{s}} N_{\mathrm{cr}}}{N_{\mathrm{y}}}\right) + \left(\frac{N_{\mathrm{cr}}}{N_{\mathrm{y}}}\right)^2 = 1 \tag{19}$$

$$N_{\mathrm{cr}} = \frac{2N_{\mathrm{y}}}{\sqrt{{k_{\mathrm{s}}}^2{\Lambda_0}^4 + 4} + k_{\mathrm{s}}{\Lambda_0}^2} \tag{20}$$

where k_{s} is a factor adopting a proposal of Kollar and Dulacska (Kollar and Dulacska 1984, Dulacska and Kollar 2000) to evaluate the axial strength of column. The magnitude of k_{s} ranges from 1.14 to 1.44 as that the column strength curves in design code are various in different countries (Dulacska and Kollar 2000). Here the k_{s} is regard as 1.2 for the column strength curve which is similar to that in AIJ LSD (Architectural Institute of Japan, 1998).

2.6.3 Evaluation of elastic-plastic buckling load of the structures

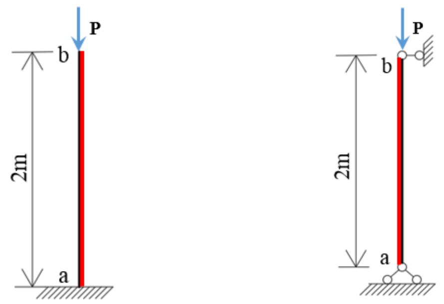

(a) Single member model-a (b) Single member model-b

Fig. 3 The boundary conditions, configurations and the load of the single members

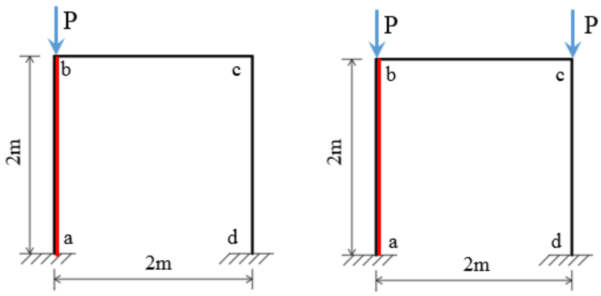

(a) Portal frame model-a (b) Portal frame model-b

Fig. 4 The boundary conditions, configurations and the loads of the portal frames

The elastic-plastic buckling load (buckling strength) of the truss structure could be evaluated by Eq. (21) based on N_{cr} (Kato 2014).

$$P_{0\mathrm{cr}} = \lambda_{\mathrm{cr}} P_0 \ \text{ or } \ q_{0\mathrm{cr}} = \lambda_{\mathrm{cr}} q_0 \tag{21}$$

$$\lambda_{\mathrm{cr}} = \frac{N_{\mathrm{cr}}}{N_0} \tag{22}$$

where P_0 and q_0 are the representative loads which have been defined in Section 2.3; N_0 is the axial force of the representative member under the representative loads P_0 or q_0; N_{cr} is the axial strength of the representative member; and $P_{0\mathrm{cr}}$ and q_{0cr} are the elastic-plastic buckling loads of the truss structure corresponding to the P_0 and q_0.

3. The buckling strength analysis of the structures under static loads

The efficiency of the proposed method is verified by analyzing the buckling strength of the single members, portal frames and simple trusses, and the above buckling strengths would be compared with the collapse loads obtained by the FEM.

3.1 Configuration of models

The single member, portal frame and simple truss with different boundaries, configurations and the loads are shown in Fig. 3 to Fig. 5, respectively. And all models are

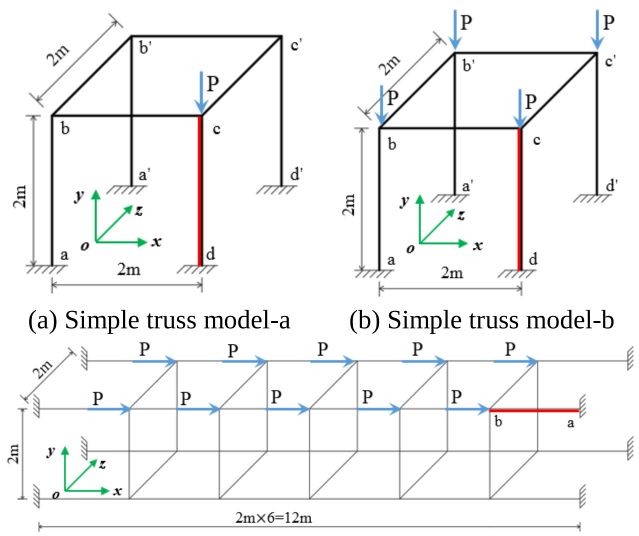

(a) Simple truss model-a (b) Simple truss model-b

(c) Simple truss model-c

Fig. 5 The boundary conditions, configurations and the loads of the simple trusses

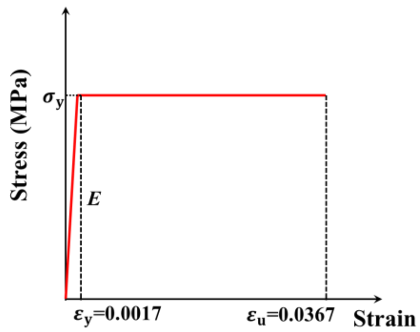

Fig. 6 Stress-strain curve for pipes

modeled in ABAQUS with beam element B31 (ABAQUS 6.13 2013, Ma *et al*. 2019). The connection in members and the boundary of all models is rigidity connection that can't rotate and displace. Moreover, all models are meshed by free meshing technology in ABAQUS. And in order to simplify the analysis, the load P is assumed to be equal to 1.00 N in all models. The pipes composing all the models are mild steel with cross-section: ϕ100×5 mm except ϕ42.4×3.5 mm for the simple truss model-c. Here, the pipes have a yield stress σ_{y} of 345 MPa, Young's modulus E of 206 GPa, and Poisson's ratio ν of 0.30. In addition, the pipes are assumed to perfect elastic-plastic material with a maximum plastic strain of 0.035 and its stress-strain curve is shown in Fig. 6.

The element B31 is based on the assumption that the deformation of the structure can be determined entirely from variables that are functions of position along the structure's length and is suitable for modeling both stout members, in which shear deformation is important, and slender beams, in which shear deformation is not important. And element B31 has six degrees of freedom at each node: translations in the nodal, *x*, *y*, and *z* directions, and rotations about the nodal *x*, *y*, and *z* axes, as shown in Fig. 7 (ABAQUS 6.13 2013).

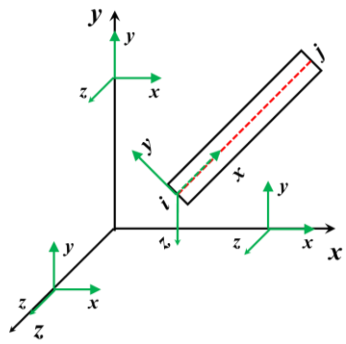

Fig. 7 Beam element geometry

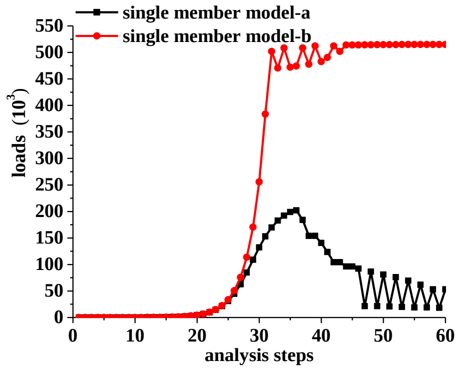

Fig. 8 The failure loads of the single member models calculated by the FEM

3.2 The buckling strength analysis of the single member

The single member model in Fig. 3, composed of only one member, will fail when the representative member fails. The representative loads P_0, loaded at node b of model-a and model-b, are both the concentrated force P. Their linear buckling strength can be calculated according to Eq. (6), Eq. (7) and Eq. (8), respectively. The main parameters of the calculation for linear buckling strength are shown in Table 1.

Here, the reduction of the buckling load, due to semi-rigid connection, is ignored as that the single member models are directly connected with supports. Namely, the parameter β equals to 1.00. The geometric imperfections of both models are assumed to be horizontal displacements in node b with amplitude w_0 of 2.00 mm according to the assumption in Section 2.5. The elastic buckling strengths of both models can be calculated according to Eq. (9), Eq. (10), Eq. (13) and Eq. (14), respectively, and their calculation are shown in Table 2.

The elastic buckling axial forces and generalized slenderness ratios of the single member model-a and model-b can be calculated according to the Eq. (16) and Eq. (17). After the calculation of generalized slenderness, the axial strengths of the single member model-a and model-b can be calculated according to Eq. (20), and their buckling strengths can be calculated by Eq. (21). The calculation for buckling strength is shown in Table 3.

To verify the proposed method, the buckling strengths of the single member model-a and model-b are also analyzed by the FEM, as shown in Fig. 8, and the results are 201.98 kN and 501.85 kN, respectively.

The ratios of the results calculated by the proposed method to that calculated by the FEM for two models are 80.32% and 76.61%, which are relatively close to each other. In addition, the results obtained by the proposed method are all lower than that calculated by FEM, the reason is that the buckling strength is corresponding to the structure buckling modes while the failure loads calculated by FEM is the structure collapse loads.

3.3 The buckling strength analysis of the portal frames

The portal frame models in Fig. 4, composed of three members, will fail when the representative member fails, because the failure of the representative member will lead to local buckling and progressive collapse of the portal frame models. Therefore, the buckling strength of the representative member can be regarded as the buckling strength of the portal frame models.

The representative member can be defined by the linear elastic analysis and the representative members a-b with red and bolded in portal frame model-a and model-b are in Fig. 4(a) and Fig. 4(b), respectively. The representative load P_0

Table 1 Calculation of linear buckling strengths for single member models

Model	$[K_E]$	$[K_s]$	$\lambda_{cr}^{lin}/(10^3)$	$N_{0cr}^{lin}/(kN)$	$P_{0cr}^{lin}/(kN)$
model-a	$\begin{bmatrix} \frac{12EI}{l^3} & \frac{6EI}{l^2} \\ \frac{6EI}{l^2} & \frac{4EI}{l} \end{bmatrix}$	$P\begin{bmatrix} \frac{6}{5l} & \frac{1}{10} \\ \frac{1}{10} & \frac{2l}{15} \end{bmatrix}$	216.12	216.12	216.12
model-b	$\begin{bmatrix} \frac{4EI}{l} & \frac{2EI}{l} \\ \frac{2EI}{l} & \frac{4EI}{l} \end{bmatrix}$	$P\begin{bmatrix} \frac{2l}{15} & -\frac{1}{30} \\ -\frac{1}{30} & \frac{2l}{15} \end{bmatrix}$	1043.26	1043.26	1043.26

Table 2 Calculation of the elastic buckling strengths for the single member models

Model	$P_{0R\_cr(imp)}^{el}$ $(\theta = 0)/kN$	$P_{0R\_cr}^{lin}$ $(\theta = 0)/kN$	α_0	β	α	$P_{0cr}^{lin}/(kN)$	λ_{0cr}^{el}	$P_{0cr}^{el}/(kN)$
model-a	216.12	216.12	1.00	1.00	1.00	216.12	216.12	216.12
model-b	1043.26	1043.26	1.00	1.00	1.00	1043.26	1043.26	1043.26

Table 3 Calculation of the buckling strength for the single member models

Model	$N_{0\mathrm{cr}}^{\mathrm{el}}/(\mathrm{kN})$	$N_{\mathrm{y}}/(\mathrm{kN})$	Λ_0	$N_{\mathrm{cr}}/(\mathrm{kN})$	$P_{0\mathrm{cr}}/(\mathrm{kN})$
model-a	216.12	514.83	1.543	162.22	162.22
model-b	1043.26	514.83	0.702	384.49	384.49

of the portal frame model-a and model-b can be respectively defined by the vertical load loaded at nodes b. Under the initial load P, the axial force N_0 of the representative member of the portal frame model-a and model-b are 0.96 N and 1.00 N, respectively.

The linear buckling strength of the representative member of the portal frame model-a and model-b can be calculated according to Eqs. (6)-(8), respectively. The calculation of the linear buckling strengths is in Table 4.

It should be noted here that the buckling load reduction due to semi-rigid connection was ignored as that the representative member of portal frame models in node a is directly supported and the semi-rigid effects in node b were considered in the materially and geometrically linear stiffness matrix $[K_{\mathrm{E}}]$ in the linear buckling analysis. Consequently, the parameter β considering the effects of semi-rigid connection can be assumed to be 1.00. However, the geometric imperfections 2.00 mm in the horizontal displacement in nodes b and c were adopted based on the assumption in Section 2.5. The elastic buckling strengths of the portal frame model-a and model-b were then calculated according to equations Eq. (9), Eq. (10), Eq. (13) and Eq. (14), respectively. The calculation process of the elastic buckling strengths is in Table 5. The elastic buckling axial forces and the generalized slenderness ratios of the portal frame model-a and model-b can be calculated by Eq. (16) and Eq. (17) as shown in Table 6. Meanwhile, Table 6 presents their axial strengths and buckling strengths

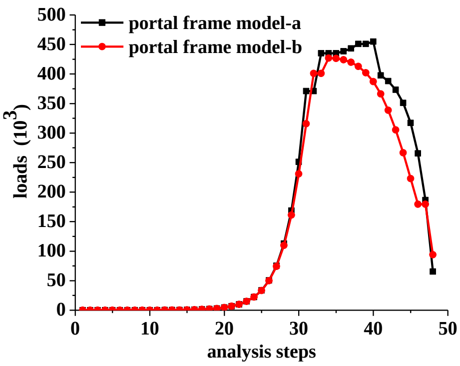

Fig. 9 The failure loads of the portal frame models calculated by the FEM

obtained by Eq. (20) and Eq. (21).

Similarly, the failure loads (454.90 kN and 426.36 kN) of the portal frame model-a and model-b were also calculated by the FEM as shown in Fig. 9 to verify the proposed method. And the ratios of the result calculated by the proposed principles to the finite element method are 88.25% and 72.47%, respectively. It is easy to see that the buckling strengths estimate by the proposed method are lower than the failure loads calculated by the FEM. The reason is that the former is related to the structure buckled state, while the latter is related to structure collapse state.

3.4 The buckling strength analysis of the simple trusses

The simple truss models in Fig. 5, composed of horizontal members and vertical members, will fail when the representative member fails, since the failure of the representative member will lead to local buckling, progressive collapse, and even a whole structure collapse.

Table 4 The linear buckling strengths of the portal frame models

Model	$[K_{\mathrm{E}}]$	$[K_{\mathrm{s}}]$	$\lambda_{\mathrm{cr}}^{\mathrm{lin}}/(10^3)$	$N_{0\mathrm{cr}}^{\mathrm{lin}}/(\mathrm{kN})$	$P_{0\mathrm{R\_cr}}^{\mathrm{lin}}/(\mathrm{kN})$	$P_{0\mathrm{cr}}^{\mathrm{lin}}/(\mathrm{kN})$
model-a	$\begin{bmatrix} \frac{24EI}{l^3} & \frac{6EI}{l^2} \\ \frac{6EI}{l^2} & \frac{4EI}{l} \end{bmatrix}$	$P\begin{bmatrix} \frac{6}{5l} & \frac{1}{10} \\ \frac{1}{10} & \frac{2l}{15} \end{bmatrix}$	1043.26	1043.26	1043.26	1043.26
model-b	$\begin{bmatrix} \frac{12EI}{l^3} & \frac{6EI}{l^2} \\ \frac{6EI}{l^2} & \frac{8EI}{l} \end{bmatrix}$	$P\begin{bmatrix} \frac{6}{5l} & \frac{1}{10} \\ \frac{1}{10} & \frac{2l}{15} \end{bmatrix}$	579.59	579.59	579.59	579.59

Table 5 The calculation of the elastic buckling strengths of the portal frame models

Model	$P_{0\mathrm{R\_cr(imp)}}^{\mathrm{el}}$ $(\theta=0)/\mathrm{kN}$	$P_{0\mathrm{R\_cr}}^{\mathrm{lin}}$ $(\theta=0)/\mathrm{kN}$	α_0	β	α	$P_{0\mathrm{R\_cr}}^{\mathrm{lin}}/(\mathrm{kN})$	$\lambda_{0\mathrm{cr}}^{\mathrm{el}}$	$P_{0\mathrm{R\_cr}}^{\mathrm{el}}/(\mathrm{kN})$	$P_{0\mathrm{cr}}^{\mathrm{el}}/(\mathrm{kN})$
model-a	1043.26	1043.26	1.00	1.00	1.00	1043.26	1043.26	1043.26	1043.26
model-b	579.59	579.59	1.00	1.00	1.00	579.59	579.59	579.59	579.59

Table 6 The buckling strengths of the portal frame models

Model	$N_{0\mathrm{cr}}^{\mathrm{el}}/(\mathrm{kN})$	$N_{\mathrm{y}}/(\mathrm{kN})$	Λ_0	$N_{\mathrm{cr}}/(\mathrm{kN})$	$N_0/(\mathrm{N})$	$\lambda_{\mathrm{cr}}/(10^3)$	$P_{0\mathrm{cr}}/(\mathrm{kN})$
model-a	1043.26	514.83	0.702	384.49	0.96	401.34	401.34
model-b	579.59	514.83	0.942	309.00	1.00	309.00	309.00

Table 7 The result of the linear elastic analysis

Model	P/N	P_0/N	N_0/N
model-a	1.00	1.00	1.05
model-b	1.00	1.00	1.00
model-c	1.00	1.00	2.67

Therefore, the buckling strength of the representative member can be regarded as the buckling strength of the simple truss models.

The representative member of the simple truss model-a, model-b and model-c can be defined by the linear elastic analysis using the finite element method according to Section 2.3, whose result are in Table 7. The representative member with red and bolded in the simple truss model-a, model-b and model-c are shown in Fig. 5(a), Fig. 5(b) and Fig. 5(c), respectively. The representative loads P_0 of the simple truss model-a, model-b and model-c can be defined by the loads directly applied at the representative member, respectively.

The axial strengths of the representative member of the simple truss model-a and model-b were 384.49 kN and 309.00 kN referring to the analysis of the portal frame model-a and model-b in Section 3.3, and their buckling strengths were 366.18 kN and 309.00 kN, respectively, given by Eq. (21) and Eq. (22). Contrastively, the results of obtained by the FEM were 454.90 kN and 426.36 kN as shown in Fig. 10. And the ratios of the results obtained by the above two methods were 80.49% and 72.47%, respectively.

Referring to the single member model-a in Fig. 3(a), the linear buckling strength of the representative member $P^{\text{lin}}_{\text{0R\_cr}}$ of the simple truss model-c is 10.44 kN, and its linear axial buckling force $N^{\text{lin}}_{\text{0cr}}$ was 10.44 kN. For the elastic buckling strength of the simple truss model-c, it must consider the effect of the geometric imperfection and semi-rigid connection. To consider the geometric imperfection, the representative member was regard as having an amplitude (w_0=12 mm) in node b which was along the y-axial and shown in Fig. 11(a), according to the assumption in Section 2.5; to considering the semi-rigid, the representative member of the simple truss model-c can be simplified as shown in Fig. 11(b), in which the stiffness of moment spring is 8*EI*/*l*, to analyze the elastic buckling strength of the simple truss model-c. Thence, the materially and geometrically linear stiffness matrix $[K_{\text{E}}]$ of the representative member of the simple truss model-c can be obtained, referring to the structural mechanics (Long *et al*. 2001), shown in Table 8. And Table 8 also presents the adjustment factor α as well as its calculation process.

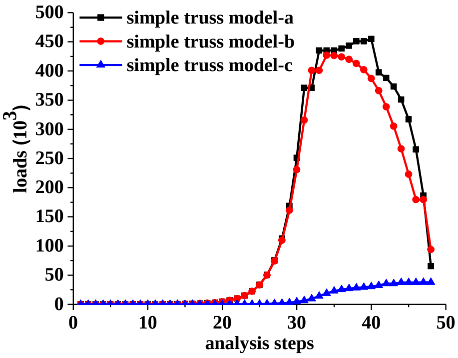

Fig. 10 The failure loads of simple truss models calculated by the FEM

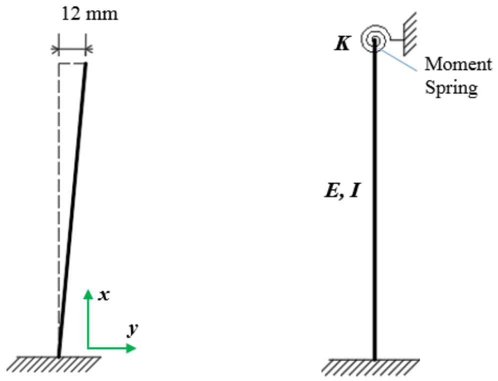

(a) Geometric imperfection (b) Semi-rigid connection

Fig. 11 The geometric imperfection and semi-rigid connection of representative member

Table 8 The elastic buckling adjustment factor α of the simple truss model-c

Model	$[K_{\text{E}}]$	$P^{\text{el}}_{\text{0R\_cr(imp)}}$ $(\theta=0)$/kN	$P^{\text{lin}}_{\text{0R\_cr}}$ $(\theta=0)$/kN	$P^{\text{el}}_{\text{0R}_{\text{cr}}}$ $(\theta=1)$/kN	$P^{\text{el}}_{\text{0R\_cr}}$ $(\theta=0)$/kN	α_0	β	α
model-c	$\begin{bmatrix} \frac{12EI}{l^3} & \frac{6EI}{l^2} \\ \frac{6EI}{l^2} & \frac{12EI}{l} \end{bmatrix}$	10.44	10.44	33.33	10.44	1.00	3.19	3.19

Table 9 The calculation of the elastic buckling strength of the simple truss model-c

Model	α	$P^{\text{lin}}_{\text{0R\_cr}}$/(kN)	$P^{\text{lin}}_{\text{0cr}}$/(kN)	$\lambda^{\text{el}}_{\text{0cr}}$	$P^{\text{el}}_{\text{0R\_cr}}$/(kN)	$P^{\text{el}}_{\text{0cr}}$/(kN)
model-c	3.19	10.44	10.44	33.33	33.33	33.33

Table 10 The calculation of the buckling strength of the simple truss model-c

Model	$N^{\text{el}}_{\text{0cr}}$/(kN)	N_y/(kN)	Λ_0	N_{cr}/(kN)	N_0/(N)	λ_{cr}/(10^3)	P_{0cr}/(kN)
model-c	33.33	147.57	2.104	26.86	2.67	10.06	10.06

Table 11 The first five natural frequency and natural period of simple truss model-c

Number	Frequency /(Hz)	Period /(s)
1	0.45	2.21
2	0.45	2.21
3	0.53	1.89
4	0.95	1.05
5	0.95	1.05

Following that, its elastic buckling strength can be calculated, shown in Table 9, by Eqs. (9)-(10) and Eqs. (13)-(14).

The elastic buckling axial force and generalized slenderness ratio of the simple truss model-c were given by Eq. (16) and Eq. (17), respectively. Following that, the axial strength and the buckling strength were obtained by Eq. (20) and Eq. (21), which are shown in Table 10.

Similarly, the failure load (41.51 kN) of the simple truss model-c analyzed by the FEM is also shown in Fig. 10. And the ratio is 24.28% between the results obtained by the proposed method and FEM. Notably, the result calculated by the proposed method is the buckling strength of the simple truss models while the FEM is the collapse load of the model. In addition, the structure buckling is earlier than collapsing.

4. The dynamic buckling strength analysis of the structure subjected to seismic load

The efficiency of the proposed method under seismic load is verified by analyzing the buckling strength of the simple truss model-c, and the maximum nodal displacement of the simple truss model-c under the buckling strength would be compared with that under seismic records.

4.1 Configuration of models

Take the truss model-c under earthquake as an example, the aim of this part is to validate the proposed method to analyze the dynamic elastic buckling load and buckling strength. The roof weight was 2 kN/m^2 and the nodal load was equivalent to the surface area supported and the lumped masses applied to the nodes are described by the point mass. Both geometrical and material nonlinearities were considered in the dynamic analysis and Rayleigh damping was assumed based on the natural periods of the first and second modes, and the damping ratio was assumed to be 0.02 (Zhang *et al*. 2018). The first five natural frequencies and periods of the simple truss model-c' are shown in Table 11.

4.2 The nodal seismic force

The general seismic force F_{Ek} of the simple truss model-c is calculated by using the response spectrum method according to the Code for Seismic Design of Buildings of China (China Architecture & Building Press 2010), as Eq. (23) shown. The simple truss model-c is assumed to be located in Doujiangyan city in Sichuan province. The characteristic period of the site T_{g} is 0.55 s and 0.60 s for frequent earthquake and rare earthquake according to the site classification (III) and classification of design earthquake (second group), and the peak ground acceleration (PGA) $A_{0\max}$ is 4.00 m/s^2 according to the seismic fortification intensity (VIII, 0.20 g) and rare earthquake in the Chinese code.

Table 12 The nodal seismic force

$m_i/(\mathrm{kg})$	$m_{\mathrm{node}}/(\mathrm{kg})$	α_1	$G_{\mathrm{eq}i}/(\mathrm{kN})$	$F_{\mathrm{Ek}i}/(\mathrm{kN})$
400	13.35	0.316	3.44	1.08

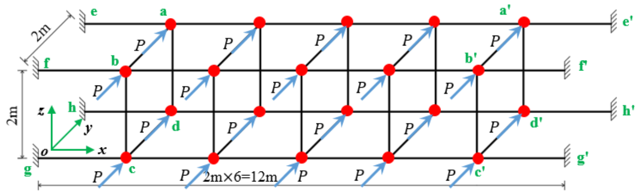

Fig.12 The seismic forces on simple truss model-c

$$F_{\mathrm{Ek}} = \alpha_1 G_{\mathrm{eq}} \tag{23}$$

where F_{Ek}, α_1 and G_{eq} denote respectively the general horizontal seismic force, the horizontal seismic influence coefficient corresponding to the structure natural period and the equivalent total gravity load of the structure which times 0.85 of the total gravity for multi-mass structure, respectively.

Here, the dynamic response analysis of the simple truss model-c under the rare earthquake needs to be carried out in order to obtain the ultimate load corresponding to the ultimate limit state. Therefore, the α_1, the equivalent total gravity load of each node in the structure $G_{\mathrm{eq}i}$, and the seismic force loaded on each node $F_{\mathrm{Ek}i}$ can be calculated by Eq. (23), listed in Table 12.

4.3 The buckling strength analysis

The elastic buckling load and buckling strength of simple truss model-c could be calculated based on the nodal seismic force $F_{\mathrm{Ek}i}$ listed in Table 12. Here, the nodal seismic force was applied along the horizontal direction as shown in Fig. 12, and the representative member can also be obtained according to its definition in Section 2.3, which is member-ae, member-dh, member-a'e' and member-d'h', and the axial force of the representative member under the unite load P is 2.79 N.

Referring to the buckling strengths analysis of the simple truss model-c in Section 3.4, the axial strength of the representative member N_{cr} is 26.86 kN. Therefore, the buckling strength $P_{0\mathrm{cr}}$, calculated by Eq. (21) and Eq. (22), is 9.63 kN, and its equivalent peak ground acceleration A_{emax} is 35.67 m/s^2, calculated by Eq. (24). The maximum nodal displacement of the simple truss model-c under the buckling strength $P_{0\mathrm{cr}}$ is 0.622 m.

$$A_{\mathrm{emax}} = \frac{P_{0\mathrm{cr}}}{F_{\mathrm{Ek}i}} A_{0\max} \tag{24}$$

Table 13 The details of the selected ground motion records

GM	NGA#	Earthquake Event	Mw	Station	Component	PGA/(m/s^2)
GM1	8	Northern Calif-01, 1941	6.40	Ferndale City Hall	FRN225	1.117
GM2	23	San Francisco, 1957	5.28	Golden Gate Park	GGP010	0.833
GM3	27	Hollister-02, 1961	5.50	Hollister City Hall	HCH181	0.568

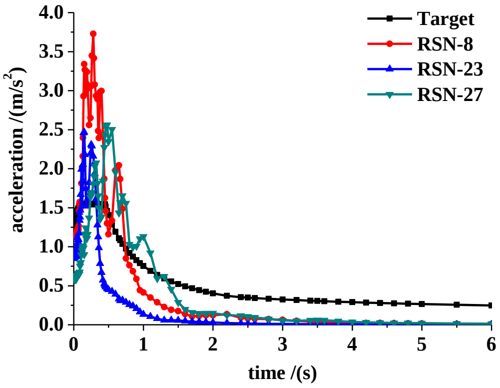

Fig. 13 The target response spectrum and response spectrum of ground motion records

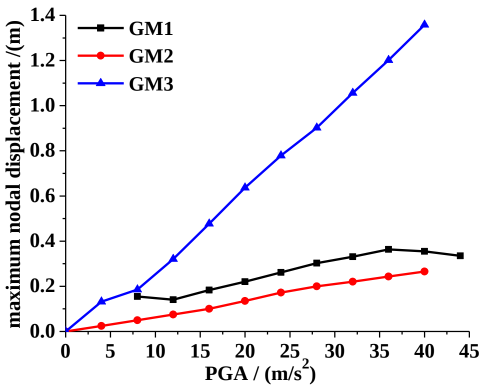

Fig. 14 The peak ground acceleration and maximum nodal displacement curves

4.4 Time history analysis by the FEM

To verify the proposed principle in the dynamic buckling strength analysis, the nonlinear dynamic time-history analysis was selected to analyze the dynamic response of the simple truss model-c. The target response spectrum of the local site in Doujiangyan city was obtained according to the Code for Seismic Design of Buildings of China (China Architecture & Building Press 2010), as shown in Fig. 13. Meanwhile, Fig. 11 also presents three response spectrums of three ground motion records selected in Pacific Earthquake Engineering Research Center in terms of the target response spectrum of the local site (Zhong *et al.* 2018). The details of three ground motion records are shown in Table 13. After that, the peak ground acceleration and maximum nodal displacement curve of the simple truss model-c were obtained, as shown in Fig. 14, by the nonlinear dynamic time-history analysis, and one of the structure deformation map of the model under GM3 is in Fig. 15.

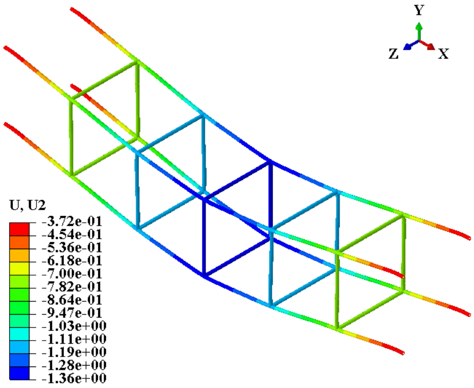

Fig. 15 The structure deformation map of the simple truss model-c under GM3

Comparing with the equivalent peak ground acceleration calculated by the proposed method, the time history analysis result is larger than it, especially, the time history analysis result under GM3 is far more than it. In addition, the result of time history analysis indicated that the deformation of the structure was too large to accept for that it has exceeded the ultimate limit states and the serviceability limit states of the structures. Significantly, the FEM analysis only gave the numerical calculation results, which can be infinitely large, and there don't have a reasonable failure criterion for truss structures, at present. Moreover, the effect of seismic records on the structure response is discrete significantly. So it is difficult to judge the failure of the structure, and this paper gives a relatively reasonable method to calculate structural failure load.

5. Conclusions

A new method is proposed to estimate the buckling strength of the truss structures based on the buckling strength of the representative member considering the structure configuration, boundary conditions, load distribution, connections between members and nodes and geometric imperfections as well as material and geometric nonlinearity. And the rationality and applicability of the new method are assessed in comparison of the FEM for estimating the buckling strength of the single members, the portal frames and the simple truss structure. The result of seismic analysis indicated that the truss structure has a good seismic performance and the effect of seismic records on the structure response is discrete significantly. The assessment indicates that the new method is feasible and reliable to estimate the buckling strengths of the truss structures under the static loads and seismic loads in terms of the results of the selected structures.

Admittedly, the proposed method is relatively conservative according to the analysis results, and further studies are required for elastic buckling load and buckling strength analysis for different truss structures. In future, a reliable dynamic failure criterion of the truss structures needs to be investigated to reasonably estimate the dynamic bearing load of the truss structures subjected different seismic records.

Acknowledgments

The present work has been conducted with the financial support from the National Natural Science Foundation of China (Grant No. 51608452). The authors also thank the financial support from IEC\NSFC\170451- International Exchanges 2017 Cost Share (China). In addition, the authors thank the anonymous reviewers and the Editors for their constructive comments and advice that helped greatly in improving the quality of this manuscript.

References

ABAQUS 6.13 (2013), Theory Reference, ABAQUS Inc..

Architectural Institute of Japan (1996), JASS6 Steel Work Japanese Architecture Standard Specification, Architectural Institute of Japan, Japan.

Architectural Institute of Japan (1998), Recommendations for Limit State Design of Steel Structures, Architectural Institute of Japan, Japan.

Architectural Institute of Japan (2010), Buckling and Strength of Latticed Shells, Architectural Institute of Japan, Architectural Institute of Japan, Japan.

Ben-Tal, A., Jarre, F., Kočvara, M., Nemirovski, A. and Zowe, J. (2000), "Optimal design of trusses under a nonconvex global buckling constraint", *Optim. Eng.*, **1**(2), 189-213.

Bi, J. (2016), "Stability analysis on large-span steel tubular truss based on finite element simulation", *International Conference on Smart Grid and Electrical Automation. IEEE*, 237-240.

China Architecture & Building Press (2010), Code for Seismic Design of Buildings, China Architecture & Building Press, China.

Dai, J., Zhe, Q., Zhang, C. and Weng, X. (2013), "Preliminary investigation of seismic damage to two steel space structures during the 2013 Lushan earthquake", *Earthq. Eng. Eng. Vib.*, **12**(3), 497-500.

Dou, C., Guo, Y.L., Zhao, S.Y., Pi, Y.L. and Braford, M.A. (2013), "Elastic out-of-plane buckling load of circular steel tubular truss arches incorporating shearing effects", *Eng. Struct.*, **52**(9), 697-706.

Dulacska, E. and Kollar, L. (2000), "Buckling analysis of reticulated shells", *Int. J. Space Struct.*, **15**(3-4), 195-203.

Halpern, A.B. and Adriaenssens, S. (2015), "Nonlinear elastic in-plane buckling of shallow truss arches", *J. Bridge Eng.*, **20**(10), 04014117.

Kato, S. (2014), "Guide to buckling load evaluation of metal reticulated roof structures", International Association for Shell and Spatial Structures.

Kollar, L. and Dulacska, E. (1984), *Buckling of Shells for Engineers*, John Wiley & Sons.

Konkong, N., Aramraks, T. and Phuvoravan, K. (2017), "Buckling length analysis for compression chord in cold-formed steel cantilever truss", *Int. J. Steel Struct.* **17**(2), 775-787.

Long, Y., Bao, S., Kuang, W. and Yuan, S. (2001), *Structural Mechanics*, Higher Education Press, Beijing, China.

Ma, Y.Y., Ma, H.H., Fan, F. and Yu, Z.W. (2019), "Experimental and theoretical analysis on static behavior of bolt-column joint under in-plane direction bending in single-layer reticulate shells", *Thin Wall. Struct.*, **135**, 472-485.

Madah, H. and Amir, O. (2017), "Truss optimization with buckling considerations using geometrically nonlinear beam modeling", *Comput. Struct.*, **192**, 233-247.

Ogawa, T., Kumagai, T., Kuruma, S. and Minowa, K. (2008), "Buckling load of elliptic and hyperbolic paraboloidal steel single-layer reticulated shells of rectangular plan", *IASS J.*, **49**(1), 31-36.

Pacific Earthquake Engineering Research Center, California, America. https://peer.berkeley.edu/

Ramesh, G. and Krishnamoorthy, C. (2005), "Inelastic post-buckling analysis of truss structures by dynamic relaxation method", *Int. J. Numer. Meth. Eng.*, **37**(21), 3633-57.

Rozvany, G.I.N. (1996), "Difficulties in truss topology optimization with stress, local buckling and system stability constraints", *Struct. Optim.*, **11**(3-4), 213-217.

Sui, Q., Lai, C. and Fan, H. (2018), "Buckling analyses of double-shell octagonal lattice truss composite structures", *J. Compos. Mater.*, **52**(9), 1227-1237.

Tada, M. and Suito, A. (1998), "Static and dynamic post-buckling behavior of truss structures", *Eng. Struct.*, **20**(4-6), 384-389.

Thai, H.T. and Kim, S.E. (2011), "Nonlinear inelastic time-history analysis of truss structures", *J. Constr. Steel Res.*, **67**(12), 1966-1972.

Tugilimana, A., Coelho, R.F. and Thrall, A.P. (2018), "Including global stability in truss layout optimization for the conceptual design of large-scale applications", *Struct. Multidisc. Optim.*, **57**(3), 1213-1232.

Wattanamankong, N., Petchsasithon, A. and Dhirasedh, S. (2017), "Analysis of lateral buckling of bar with axial force accumulation in truss", *IOP Conference Series: Materials Science and Engineering*, **216**(1), 012037.

Zhang, M., Parke, G., Tian, S., Huang, Y. and Zhou, G. (2018) "Criterion for judging seismic failure of suspen-domes based on strain energy density", *Earthq. Struct.*, **15**(2), 123-132.

Zhang, Q., An, Y., Zhao, Z., Fan, F. and Shen, S. (2019), "Model selection for super-long span mega-latticed structures", *J. Constr. Steel Res.*, **154**, 1-13.

Zhong, J., Zhang, J., Zhi, X. and Fan, F. (2018) "Identification of dominant modes of single-layer reticulated shells under seismic excitations", *Thin Wall. Struct.*, **127**:676-687.

CC